

Preparation of Polyaniline/Epoxy Composite and Its Anti-Corrosion Performance

Qianqian Wang

Civil Engineering College, Zhengzhou University of Technology, Zhengzhou, Henan 450000, China
E-mail: wqqqianqianw@163.com

Received: 21 November 2021 / *Accepted:* 11 January 2022 / *Published:* 4 March 2022

Anti-corrosion coatings are an effective method of reducing material surface corrosion and have been extensively studied as a result. Polyaniline is a novel type of polymer material that exhibits low cost, excellent chemical and thermal stability, ease of synthesis, and high anti-corrosion properties. Epoxy resin, another key component, exhibits excellent adhesion, strength, chemical resistance, and wear resistance. We attempted to combine the excellent film-forming properties of epoxy resin with the anti-corrosion properties of polyaniline in this study in order to create functional coatings with enhanced anti-corrosion properties. Polyaniline/epoxy composite coatings with various polyaniline additions were prepared in this work, with polyaniline additions of 0%, 1%, 2%, and 4%. EIS was used for 11 days to determine the impedance and capacitive resistance spectra of the various coatings. When the control realities are compared, it is clear that the coating with a 2% addition has significantly better anticorrosive performance than the other samples.

Keywords: Polyaniline, Epoxy resin, Anti-corrosion, Coating, EIS

1. INTRODUCTION

Corrosion of metals is a phenomenon in which metals and their surrounding media are harmed through physical, chemical, or electrochemical interaction. To resolve the problem of metal corrosion, it is necessary to maintain the metal in a stable state, allowing it to perform its intended function and effect [1–3]. As a result, take a variety of protective measures to minimize the production and development of rotten candle. In general, there are four distinct types of protection: (1) processing products with relatively stable metal and alloy materials [4–7]; (2) plating non-metal and metal surfaces, forming a protective layer on the metal surface, and sealing the metal to isolate it from the outside [8–10]; (3) in the case of corruption, researching the product of corruption candle and altering its properties, reducing harmful components, in order to achieve an anti-corrosion effect [11–13]; (4) using straight

metal and alloy materials. The current modifies the metal's potential to slow or stop the corrosion reaction [14–17].

Among the four methods discussed above, coating technology is particularly significant as a means of corrosion and protection [18–21]. Corrosion of the metal covered by the coating is directly related to the coating's performance. The bond strength between the coating and the metal matrix, the coating's resistance to water and other corrosive particles, the metal matrix's surface properties and pretreatment status, the composition and structure of the organic coating, and a variety of other factors, such as the coating metal's ambient temperature, all have a significant effect on the coating's service life and protective performance [22–25]. Due to the inherent limitations of traditional coating materials and processing technologies, the corrosion protection effect of traditional coatings on base metals is frequently suboptimal [26–28]. A significant portion of traditional coatings contain toxic substances such as lead and chromate, which are hazardous during the preparation and use processes. As a result, the development of new coatings that are high performing, low polluting, and multifunctional has become a focus of research in recent years [29–31].

The most effective anticorrosive coatings available today are hexavalent chromium and lead compounds [32,33]. Hexavalent chromium, on the other hand, is a carcinogen, and lead is a heavy metal that contributes significantly to environmental pollution [34,35]. Numerous countries worldwide are looking for non-toxic and low-toxic alternatives, and polyaniline is an excellent choice as an environmentally friendly and highly effective anti-corrosion coating material. Polyaniline is produced chemically or electrochemically by polymerizing aniline monomer. Polyaniline can be used to purify metal, and the cathodic reaction occurs on polyaniline rather than at the coating-metal interface. The reaction between the anode and cathode occurs in distinct spaces to maintain the passivation state [36–38]. Additionally, some researchers believe that proton acid ions, such as phosphate, can form an insoluble composite protective layer on the metal surface, effectively passivating it. Polyaniline and steel surfaces, for example, formed an intermediate between oxidized polyaniline and dense film [39–41]. Because polyaniline has a higher redox potential than iron, it reacts preferentially with oxygen in the air to form intermediate oxidized polyaniline in a water environment. The intermediate oxidation state reacts with the surface iron, resulting in the reduction of polyaniline oxide. A polyaniline coating on the metal surface generates an electric field in the opposite direction of the electrons produced by metal oxidation, effectively preventing or significantly ameliorating metal corrosion.

Polyaniline, a mass-produced anti-corrosion filler, was used as the anti-corrosion filler in this paper, while epoxy resin, a widely used base resin, was used as the anti-corrosion filler. This work discusses the amount of polyaniline to be added, determines the optimal amount, and finally develops a production-ready coating formulation.

2. EXPERIMENTAL

2.1 Reagents and instruments

The epoxy resin (E-44) was purchased from Zhenjiang Danbo Resin Co. T31 curing agent was purchased from Kunshan Beiya Chemical Co. Polyaniline was purchased from Cornell Chemical Co. All other reagents were analytical grade and used without further purification.

A scanning electron microscope was used to examine the surface morphology (SEM, SSX-550, SHIMADZU Corp.). A X-ray diffractometer was used to record the XRD pattern (Empyrean, PANalytical B.V.). Nicolet Impact 410 is a Fourier Transform Infrared Spectroscopy (FTIR) instrument. A PARSTAT 2273 workstation was used to conduct the electrochemical impedance spectroscopy test (AMETEK). The test was conducted with a 1 mV voltage amplitude and a test frequency ranging from 0.01 Hz to 100 KHz. The initial voltage was that of an open circuit. A three-electrode system was used, consisting of a platinum auxiliary electrode, a saturated potassium chloride reference electrode, and a composite coating/steel plate working electrode. A 3.5% mass fraction sodium chloride solution was used as the corrosion medium.

2.2 Preparation of coatings

The coatings examined in this section were solvent-based, and it is necessary to thoroughly mix the film-forming resin, fillers, film-forming additives, and mixed solvents to achieve a uniformly dispersed coating. The primary preparation procedure is as follows: the resin is weighed and added to the grinding tank along with the mixed solvent. To create a uniform resin solution, the toothed rotating head is mounted on the stirring sand mill disperser and stirred at 1000 revolutions per minute for 10 minutes. The toothed stirring head was removed and a tetrafluoroethylene sanding and dispersing disc was installed in its place. The grinding tank was then filled with zirconium beads, and fillers and additives were added sequentially while stirring at a rate of 2000 r/min and then increased to 3500-4000 r/min for 6 hours. The filtered coating was stored in an airtight plastic jar. In this work, polyaniline/epoxy composite coatings (designated PANI-1, PANI-1, PANI-2, and PANI-4) with polyaniline additions of 1%, 2%, and 4% were prepared (polyaniline addition refers to the proportion of polyaniline in addition to the curing agent in this paper). The coatings' specific composition is listed in Table 1. The solvent was xylene:n-butanol=4:3, 1 g titanium dioxide was added, and 0.5 g carbon black was added.

Table 1. Coating formulation.

Component	PANI-0	PANI-1	PANI-2	PANI-4
Epoxy (g)	160	160	160	160
PANI (g)	0	1.70	3.40	6.80
Anti-settling pulp (g)	100	100	100	100
Solvents (g)	40	40	40	40

2.3 Spraying of coatings

The steel plate used in the experiment was manufactured by Q-PANEL of the USA, model R-2-3.5. Q-PANEL steel test substrates have been recognized as the world standard for a uniform and consistent test surface for paints, adhesives, sealants, and other coatings. The model R-2-3.5. is a dull matte mill finish produced by roughened rolls. This matte finish is representative of general purpose sheet metal applications. Table 2 shows the information of used steel plate. To improve the coating's

adhesion to the steel plate's surface, the steel plate must be sandblasted prior to spraying. After sandblasting, clean the steel plate with acetone and ethanol and then dry it before use. Due to the fact that the viscosity of the liquid coating has a significant effect on the coating thickness and other properties, it is necessary to measure the viscosity of the coating each time it is used. The viscosity is measured in accordance with GB/T1723-1993, and the coating is generally adjusted to a viscosity of about 40-50 s.

Table 2. Information of R-2-3.5 steel plate.

SAE Material Designation	1008/1010	ASTM Material Specifications	A1008
ISO Material Specifications	3574 Type CR1	ASTM Panel Specifications	D609 -Type 1
ISO Panel Specifications	1514-Type 1	Roughness Ra (micro-inches)	25-65
Surface Finish	Dull Matte	Temper	1/4 hard
Hardness (Rockwell)	B50-B65	Tensile Strength (kpsi)	45-65
Tensile Strength (MPa)	310-448		

3. RESULTS AND DISCUSSION

The SEM picture of polyaniline in Figure 1 demonstrates that the particles are organized irregularly. The particle size ranges between 3-5 m, and the particle size distribution is rather consistent. This microscopic structure facilitates dispersing and filling the faults and micro-pores in the epoxy coating, thereby reducing defects, increasing the coating's density, and increasing the coating's corrosion resistance. However, because polyaniline is agglomerative, it should be ground thoroughly to prevent polyaniline agglomeration from generating coating flaws.

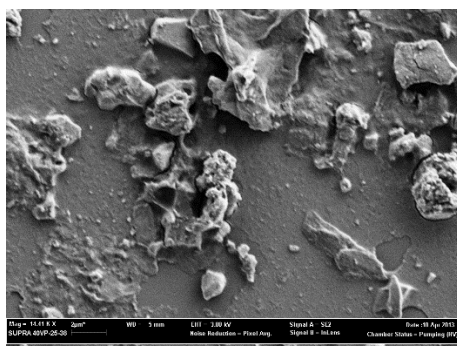


Figure 1. Scanning electron microscope image of polyaniline.

Figure 2A shows the infrared spectrum of polyaniline, from which it can be seen that polyaniline has absorption peaks at wave numbers 1581 cm^{-1} , 1490 cm^{-1} , 1307 cm^{-1} , 1149 cm^{-1} and 828 cm^{-1} . These are the characteristic absorption peaks of polyaniline.

The X-ray diffraction pattern of polyaniline is shown in Figure 2B. Polyaniline has enlarged crystalline peaks at $2\theta=15.5^\circ$, 20° , and 24° . 15.5° corresponds to the (011) crystal plane of polyaniline in its emerald green imine salt form, 20° to the (020) crystal plane of polyaniline in its emerald green imine salt form, and 24° to the (200) crystal plane of polyaniline in its emerald green imine salt form. This suggests that the polyaniline utilized in this article is a lattice-formed organic polymer with long-range organization.

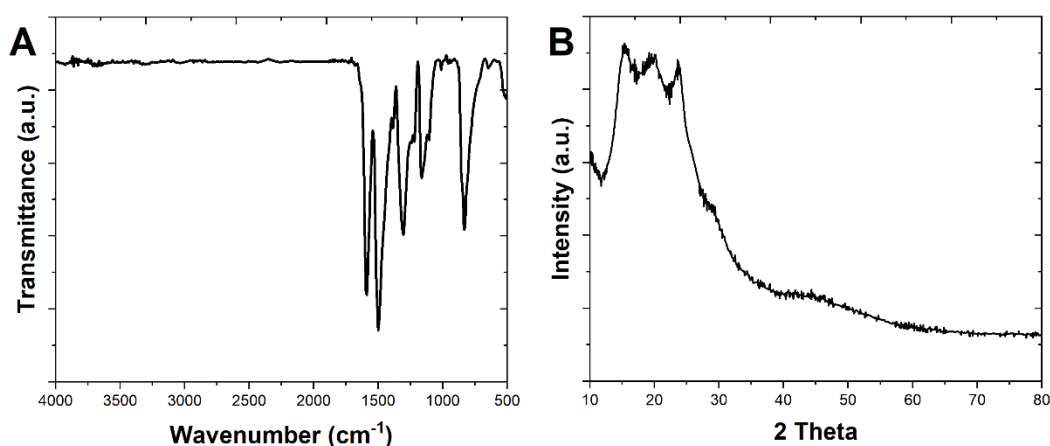


Figure 2. (A) Infrared spectra of polyaniline. (B) X-ray diffraction pattern of polyaniline.

The open-circuit voltage of each coating was determined as a function of immersion time using the three-electrode technique, and the findings are displayed in Figure 3. The horizontal coordinate of the graph reflects the number of days that the three-electrode system was immersed in a 3.5% chlorinated steel aqueous solution, and the vertical coordinate indicates the working electrode's stable open-circuit voltage as measured.

The open-circuit potential is the difference between the potentials of the working electrode and the reference electrode in the absence of a load [42,43]. The change in open circuit voltage is indicative of the electrode's transition from unstable to stable. The open-circuit potential method's purpose is to determine the stability of the working electrode voltage over time. In the case of coating systems, the open circuit potential can be utilized to determine the coating's initial effectiveness [44]. As illustrated in Figure 3, the open circuit potential of PANI-0 tends to flatten out after three days and is close to the corrosion potential of R-2-3.5, indicating that the risk of failure is rather high. In comparison, the open circuit potentials of PANI-1, PANI-2, and PANI-4 are further from R-2-3.5, implying that the coating is still effective.

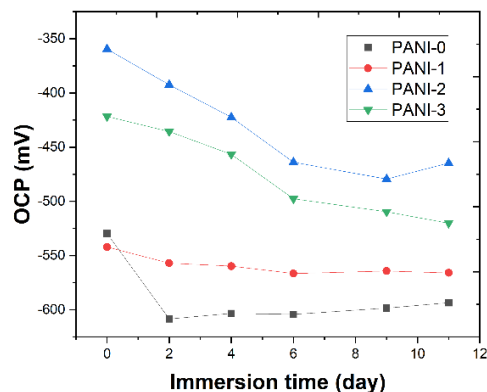


Figure 3. Variation of open circuit potential of 3.5% NaCl aqueous solution coating with immersion time.

The three-electrode system was used to determine the polarization curves of each coating, and the findings are displayed in Figure 4. The polarization curve is the connection between the polarization current density and the electric trigger potential. The corrosion potential and current of the coating can be determined from the polarization curve. Table 3 summarizes the findings. The corrosion potential is the potential formed when a substance is immersed in a medium without conducting current [45]. Even when the electrode's net current is zero, a corrosion potential exists since the corrosion reaction continues at a predetermined rate. At this point, the anodic and cathodic currents are equal in magnitude and direction and equal to a specified current value. The current value represents the corrosion current of the electrode. The corrosion potential of a coating indicates the coating's thermodynamic state. In general, the higher the corrosion potential of the coating, the greater its corrosion resistance [46,47]. The corrosion current of the coating indicates the coating's kinetic state, and the magnitude of the corrosion current value indicates the rate of deterioration. As the table indicates, PANI-2 has the highest corrosion potential and the lowest corrosion current, indicating that it has the best anti-corrosion ability. Additionally, as shown in Table 3, an excessive amount of PANI has poor anti-corrosion characteristics.

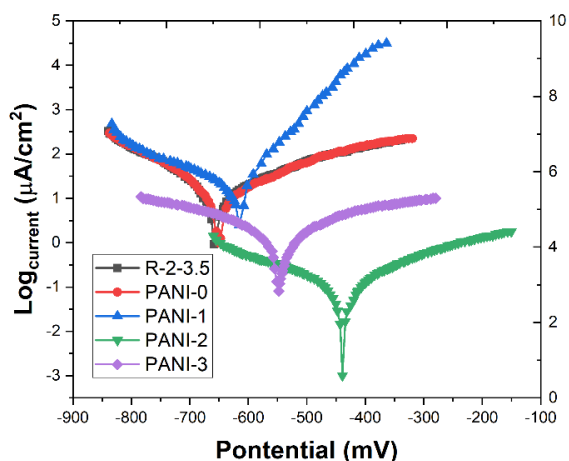


Figure 4. Polarization curves of coating systems immersed in 3.5% aqueous sodium chloride solution at a scan rate of 0.15 mV/s vs. Ag/AgCl (KCl sat.) reference electrode.

The three-electrode system was utilized to determine the Nernst and Bode spectra of each coating system over a range of immersion periods in this investigation. The most often used impedance spectra are the Nernst and Bode spectra. The Nernst spectrum reflects the relationship between the impedance's real and imaginary components. The Bode spectrum is a representation of the connection between frequency and impedance's absolute value.

Table 3. Corrosion potential and corrosion current of different coatings.

Coating	R-2-3.5	PANI-1	PANI-2	PANI-4	Epoxy
Corrosion potential (mV)	-650	-516	-434	-618	-651
Corrosion current (μA)	20.51	7.14	0.23	25.14	20.21

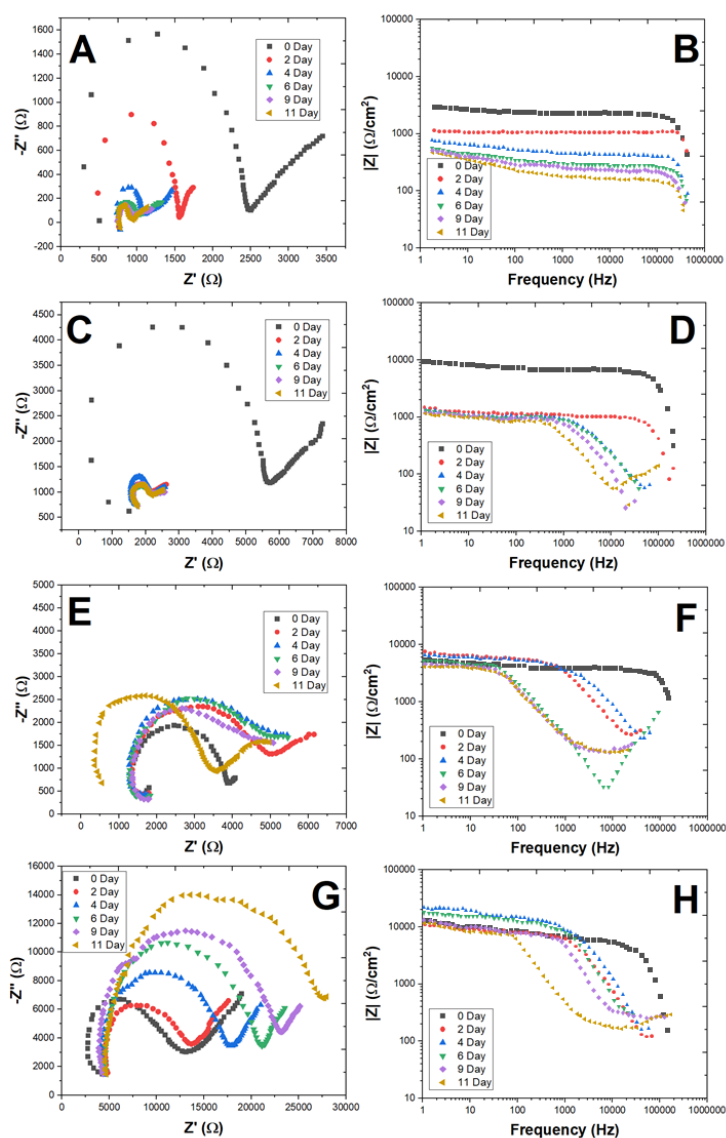


Figure 5. EIS profiles of (A,B) PANI-0, (C,D) PANI-1, (E,F) PANI-2 and (G,H) PANI-3 at different immersion times from 1 M Hz to 0.01 Hz.

The capacitive arc diameter in the high frequency zone characterizes the charge transfer resistance of the coating in an electrode system with mixed control of charge transfer and diffusion processes. The Nernst figure in Figure 5A shows that as the immersion time increases, the capacitive arc in the high-frequency area decreases [48,49]. This suggests that the coating's charge transfer resistance gradually declines, implying a reduction in corrosion resistance. At low frequencies, the impedance modulus can be used to quantify the coating's anticorrosive capabilities [50]. The Bode curve in Fig. 5B demonstrates that as immersion duration increases, the impedance at 1 Hz diminishes, indicating that the coating gradually loses its corrosion resistance to corrosive ions (e.g., chloride ions, etc.). As illustrated in Figures 5C and 5D, the PANI coating exhibits a comparable electrochemical impedance behavior to that of the epoxy resin coating. The coating exhibits some corrosion resistance during the initial stages of immersion, but after three days of immersion, corrosion resistance rapidly declines or even fails. As illustrated in Figure 4E, PANI-1 retains some anticorrosive capabilities after 11 days of immersion. The charge transfer resistance of the coating system is roughly 4 k after 11 days of immersion, and the $|Z|$ value at 1 Hz ranges between 1000 and 10000 Ω/cm^2 . When illustrated in Figure 5G-H, PANI-2 has the best anticorrosive performance of all coating systems, and as the number of days of immersion increases, anticorrosive performance exhibits a progressive improvement in trend. According to Figure 5G, the charge transfer resistance of the coating after 11 days of immersion is around 27 k/cm, and the Z value of the system at 1 Hz is between 10–100 k/cm.

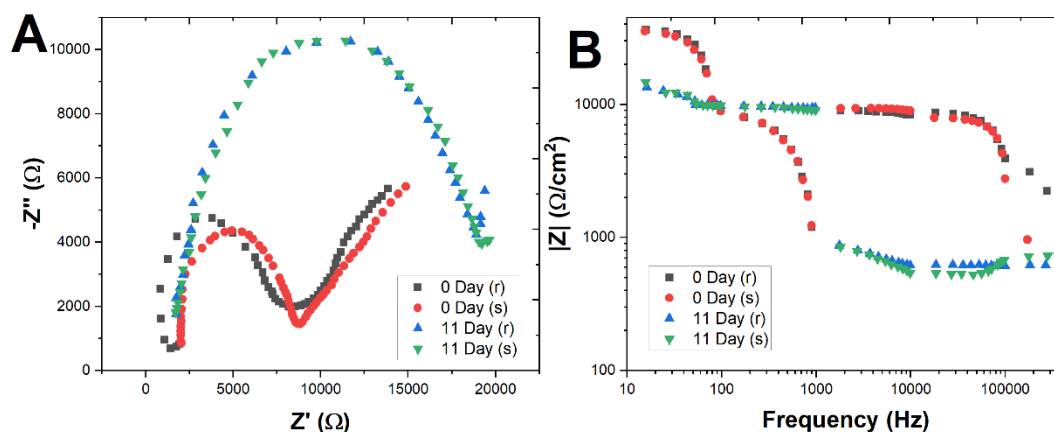


Figure 6. (A) Measured and fitted Nernst spectra of PANI-2 coatings at different immersion times. (B) Measured and fitted values of the Bode spectra of PANI coatings at different immersion times from 1 M Hz to 0.01 Hz.

Table 4. Impedance data of PANI-0, PANI-1, PANI-2 and PANI-3 calculated using equivalent-circuit diagram.

Immersion time	R_{Ω} (Ω)	C_d (μF)	$R_{CT} + R_w$ (Ω)	C_w (μF)
PANI-0-0 day	1×10^{-7}	4.511×10^{-3}	1.014×10^3	14.07
PANI-0-11 day	3×10^{-5}	2.615	4.501×10^4	22.21
PANI-1-0 day	1×10^{-7}	2.147×10^{-4}	2.014×10^2	17.56
PANI-1-11 day	2×10^{-6}	7.066×10^{-1}	1.047×10^4	20.21

PANI-2-0 day	1×10^{-7}	7.214×10^{-4}	1.022×10^4	16.77
PANI-2-11 day	1×10^{-7}	2.031×10^{-1}	2.124×10^4	25.59
PANI-3-0 day	1×10^{-6}	4.017×10^{-4}	4.147×10^4	18.18
PANI-3-11 day	3×10^{-5}	1.414	1.077×10^3	14.61

The results from the PANI-2 EIS experiment were fitted using an analogous circuit, and the difference between the present and calculated curves is displayed in Figure 6. Where (r) denotes the measured value and (s) denotes the fitted value. Table 4 contains the fitted values for each electronic component. For all four samples, R increased as the immersion time increased. In the presence of PANI, the corrosion reaction's charge transfer was inhibited, resulting in an increase in corrosion resistance.

4. CONCLUSION

This work characterized PANI and created polyaniline/epoxy composite coatings with various polyaniline amounts of 1%, 2%, and 4%, respectively. EIS experiments were performed on the coatings in a 3.5 percent NaCl solution. The selected polyaniline particle size was determined to be between 2 and 5 m. Chemical stability was demonstrated by IR and XRD measurements. EIS measurements were used to determine the impedance and capacitive resistance spectra of the various coatings with varying amounts of polyaniline composite coatings during an 11-day period. The comparative comparison demonstrates that PANI-2 has much superior anticorrosive properties to the other samples. The anticorrosive coating developed in this study is a simple method that is environmentally friendly. Due to its outstanding anticorrosive properties in 3.5 percent NaCl aqueous solution, it has prospective applications in the field of anticorrosion, particularly maritime anticorrosion.

ACKNOWLEDGEMENTS

This work was supported by The key project of the school-level and Zhengzhou local college education and teaching reform project 'Exploration of the collaborative construction of engineering education certification and new engineering in new undergraduate colleges' (ZZJG-A9003) and School-level key discipline 'Disaster prevention and mitigation engineering and protection engineering'.

References

1. S.A. Umoren, U.M. Eduok, *Carbohydr. Polym.*, 140 (2016) 314–341.
2. R. Asri, W. Harun, M. Samykano, N. Lah, S. Ghani, F. Tarlochan, M. Raza, *Mater. Sci. Eng. C*, 77 (2017) 1261–1274.
3. S.A. Umoren, M.M. Solomon, *J. Environ. Chem. Eng.*, 5 (2017) 246–273.
4. C. Verma, L.O. Olasunkanmi, E.E. Ebenso, M.A. Quraishi, I.B. Obot, *J. Phys. Chem. C*, 120 (2016) 11598–11611.
5. N. Wang, Y. Zhang, J. Chen, J. Zhang, Q. Fang, *Prog. Org. Coat.*, 109 (2017) 126–134.
6. M. Cabrini, S. Lorenzi, T. Pastore, S. Pellegrini, D. Manfredi, P. Fino, S. Biamino, C. Badini, *J. Mater. Process. Technol.*, 231 (2016) 326–335.
7. Y.M. Panchenko, A. Marshakov, *Corros. Sci.*, 109 (2016) 217–229.

8. M. Belghiti, S. Echihi, A. Dafali, Y. Karzazi, M. Bakasse, H. Elalaoui-Elabdallaoui, L. Olasunkanmi, E. Ebenso, M. Tabyaoui, *Appl. Surf. Sci.*, 491 (2019) 707–722.
9. P.B. Raja, M. Ismail, S. Ghoreishiamiri, J. Mirza, M.C. Ismail, S. Kakooei, A.A. Rahim, *Chem. Eng. Commun.*, 203 (2016) 1145–1156.
10. F.E.-T. Heakal, A.E. Elkholy, *J. Mol. Liq.*, 230 (2017) 395–407.
11. S. Kim, T.-H. Le, C.S. Park, G. Park, K.H. Kim, S. Kim, O.S. Kwon, G.T. Lim, H. Yoon, *Sci. Rep.*, 7 (2017) 15184.
12. J. De Damborenea, M. Arenas, M.A. Larosa, A.L. Jardini, C.A. de Carvalho Zavaglia, A. Conde, *Appl. Surf. Sci.*, 393 (2017) 340–347.
13. M. Deyab, *Desalination*, 384 (2016) 60–67.
14. D. Di Marino, M. Shalaby, S. Kriescher, M. Wessling, *Electrochem. Commun.*, 90 (2018) 101–105.
15. S. Javadian, B. Darbasizadeh, A. Yousefi, F. Ektefa, N. Dalir, J. Kakemam, *J. Taiwan Inst. Chem. Eng.*, 71 (2017) 344–354.
16. S. Qiu, C. Chen, W. Zheng, W. Li, H. Zhao, L. Wang, *Synth. Met.*, 229 (2017) 39–46.
17. A. Singh, I. Ahamad, M.A. Quraishi, *Arab. J. Chem.*, 9 (2016) S1584–S1589.
18. M. Ates, *J. Adhes. Sci. Technol.*, 30 (2016) 1510–1536.
19. E. Vazirinasab, R. Jafari, G. Momen, *Surf. Coat. Technol.*, 341 (2018) 40–56.
20. H.-S. Lee, J. Singh, M. Ismail, C. Bhattacharya, *Metals*, 6 (2016) 55.
21. J. Wang, Y. Song, J. Wang, Q. Zhou, Z. Li, Y. Han, S. Yang, G.L. Li, T. Qi, *Macromol. Mater. Eng.*, 302 (2017) 1700128.
22. K.J. Ma, J. Stankus, D. Faulkner, *Int. J. Min. Sci. Technol.*, 28 (2018) 145–151.
23. J. Wu, C. Cai, Z. Zhou, H. Qian, F. Zha, J. Guo, B. Feng, T. He, N. Zhao, J. Xu, *J. Colloid Interface Sci.*, 463 (2016) 214–221.
24. Y. Hao, L.A. Sani, T. Ge, Q. Fang, *Appl. Surf. Sci.*, 419 (2017) 826–837.
25. G.-C. Son, D.-K. Hwang, J. Jang, S.-S. Chee, K. Cho, J.-M. Myoung, M.-H. Ham, *Nano Res.*, 12 (2019) 19–23.
26. Z. Grubač, I.Š. Rončević, M. Metikoš-Huković, *Corros. Sci.*, 102 (2016) 310–316.
27. N. Parhizkar, B. Ramezanzadeh, T. Shahrabi, *Appl. Surf. Sci.*, 439 (2018) 45–59.
28. A. Gnedenkov, S. Sinebryukhov, D. Mashtalyar, S. Gnedenkov, *Corros. Sci.*, 102 (2016) 269–278.
29. J. Mosa, N. Rosero-Navarro, M. Aparicio, *RSC Adv.*, 6 (2016) 39577–39586.
30. W. Sun, L. Wang, T. Wu, Y. Pan, G. Liu, *J. Electrochem. Soc.*, 163 (2016) C16–C18.
31. A. Adhikari, R. Karpoornath, S. Radha, S.K. Singh, R. Mutthukannan, G. Bharate, M. Vijayan, *High Perform. Polym.*, 30 (2018) 181–191.
32. O. Dagdag, O. Hamed, H. Erramli, A. El Harfi, *J. Bio-Tribo-Corros.*, 4 (2018) 52.
33. C.-H. Lin, C.-H. Lai, Y.-P. Peng, P.-C. Wu, K.-Y. Chuang, T.-Y. Yen, Y.-K. Xiang, *Environ. Sci. Pollut. Res.* (2018) 1–11.
34. P. Rivero, D. Yurrita, C. Berlanga, J. Palacio, R. Rodríguez, *Coatings*, 8 (2018) 300.
35. C. Zea, R. Barranco-García, J. Alcántara, B. Chico, M. Morcillo, D. de la Fuente, *J. Coat. Technol. Res.*, 14 (2017) 869–878.
36. F. Xiao, C. Qian, M. Guo, J. Wang, X. Yan, H. Li, L. Yue, *Prog. Org. Coat.*, 125 (2018) 79–88.
37. M.G. Hosseini, K. Aboutalebi, *Synth. Met.*, 250 (2019) 63–72.
38. P. Du, C. Liu, S. Qiu, G. Liu, H. Zhao, *Surf. Topogr. Metrol. Prop.*, 6 (2018) 034012.
39. A. Saikia, D. Sarmah, A. Kumar, N. Karak, *J. Appl. Polym. Sci.*, 136 (2019) 47744.
40. C.M.D.L. Almazán, M.Y. Chávez-Cinco, U. Páramo-García, A.M. Mendoza-Martínez, I.A. Estrada-Moreno, J.L. Rivera-Armenta, *Polym. Bull.*, 73 (2016) 1595–1605.
41. J. Iribarren, M. Català, A.J. Conchello, M. Pérez-Madrigal, C. Alemán, *Surf. Eng. Appl. Electrochem.*, 54 (2018) 297–306.

42. H. Karimi-Maleh, Y. Orooji, F. Karimi, M. Alizadeh, M. Baghayeri, J. Rouhi, S. Tajik, H. Beitollahi, S. Agarwal, V.K. Gupta, *Biosens. Bioelectron.* (2021) 113252.
43. H. Karimi-Maleh, A. Khataee, F. Karimi, M. Baghayeri, L. Fu, J. Rouhi, C. Karaman, O. Karaman, R. Boukherroub, *Chemosphere*, (2021) 132928.
44. Z. Zhang, M. Peng, D. Li, J. Yao, Y. Li, B. Wu, L. Wang, Z. Xu, *Front. Chem.*, 9 (2021) 702.
45. H. Karimi-Maleh, F. Karimi, L. Fu, A.L. Sanati, M. Alizadeh, C. Karaman, Y. Orooji, *J. Hazard. Mater.*, 423 (2022) 127058.
46. Y. Yue, L. Su, M. Hao, W. Li, L. Zeng, S. Yan, *Front. Chem.*, 9 (2021) 479.
47. S. Yan, Y. Yue, L. Zeng, L. Su, M. Hao, W. Zhang, X. Wang, *Front. Chem.*, 9 (2021) 220.
48. W. Li, W. Luo, M. Li, L. Chen, L. Chen, H. Guan, M. Yu, *Front. Chem.*, 9 (2021) 610.
49. Y. Wang, L. Chen, T. Xuan, J. Wang, X. Wang, *Front. Chem.*, 9 (2021) 569.
50. R. Duan, X. Fang, D. Wang, *Front. Chem.*, 9 (2021) 361.

© 2022 The Authors. Published by ESG (www.electrochemsci.org). This article is an open access article distributed under the terms and conditions of the Creative Commons Attribution license (<http://creativecommons.org/licenses/by/4.0/>).